Probing dark matter distribution with galaxy-galaxy lensing

Zuhui Fan
Dept. of Astronomy, Peking University

Outline:

- Introduction
- Galaxy-galaxy lensing effects
- Probing the subhalo properties with g-g lensing

Introduction

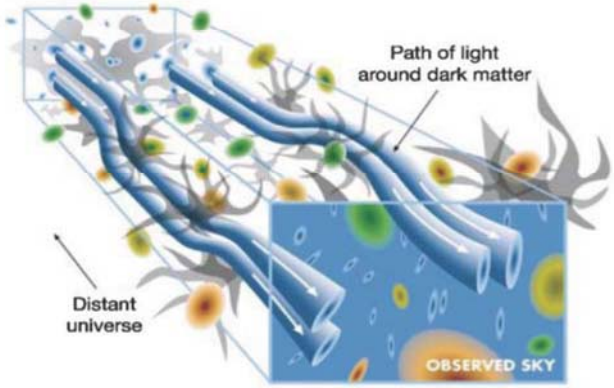

Weak lensing effects

Weak distortions/magnifications caused by large-scale structures of the universe: common but weak

- powerful probe for the large-scale distribution of dark matter

- sensitive to the formation of large-scale structures and the global geometry of the universe

→ highly promising in dark energy studies

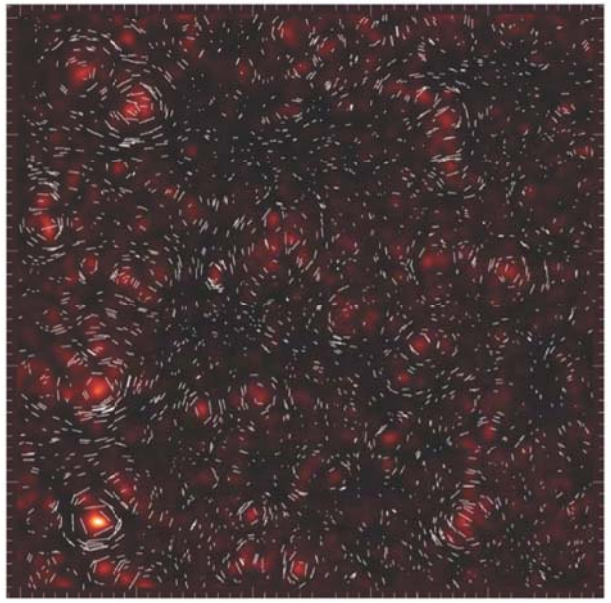

Map out the mass distribution of the universe

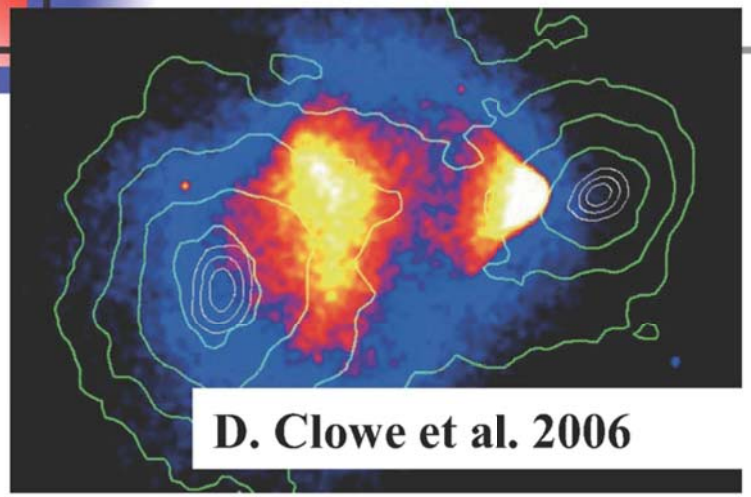

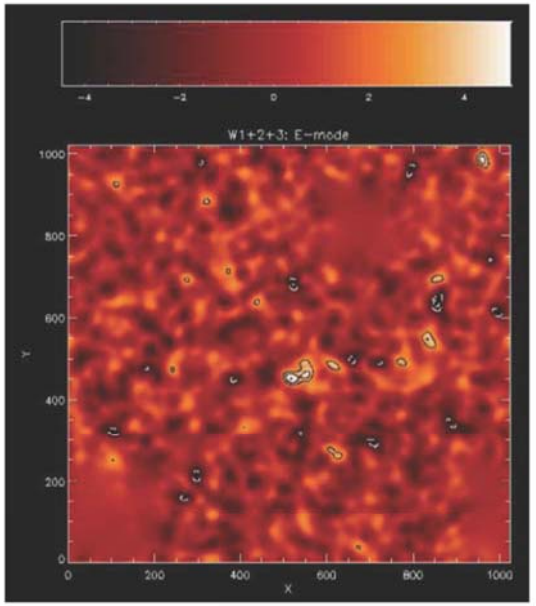

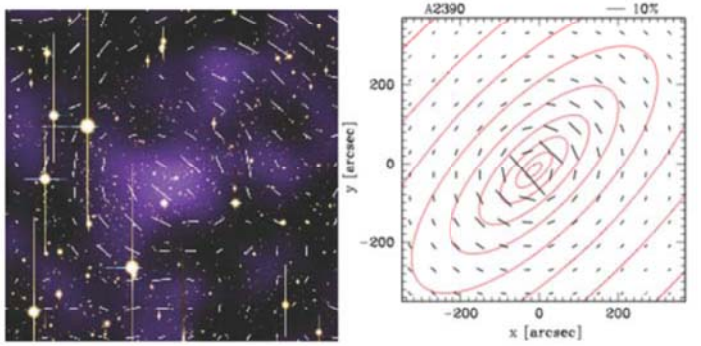

Figure 1. *Left panel:* An example of our weak lensing measurement for A2390. The size of Each panel is $12' \times 12'$. The stick in each $1' \times 1'$ pixel shows the distortion field estimated from background galaxy images contained within the pixel, where a background galaxy image is deformed along the stick direction, and the length is proportional to the shear amplitude. The shear field in this panel is smoothed with a Gaussian with the full width at half maximum of $\simeq 1.6'$ for illustrative purpose. Overplotted is the surface mass density map reconstructed from the weak lensing shear measurement (see Okabe et al. 2010). North is up and East is left. *Right panel:* The shear field predicted by our best-fit elliptical NFW model (see also Figure 2 and Table 1), while the contours are the isodensity map. The best-fit ellipticity of the projected mass density is $e \equiv 1 - b/a = 0.598$.

Oguri et al. 2010, Okabe et al. 2009

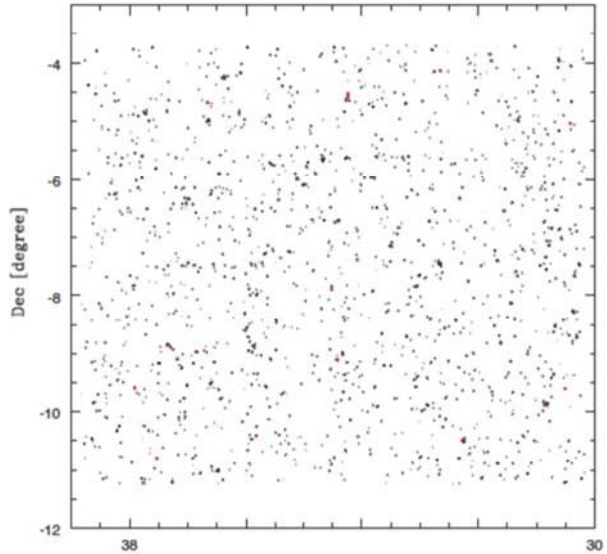

Shan et al. 2011

Figure 12. Reconstructed "dark
The lowest contour is drawn at de
red contours denote $\nu \geq 4.5$.

SKLTP

Cosmological constraints from cosmic shear analyses

Fu et al. 2008 A&A (CFHTLS)

Li, H. et al. 2009 (RCS, VIRMOS,GaBoDS,CFHTLS(22)
total ~100deg*deg, varying depth)

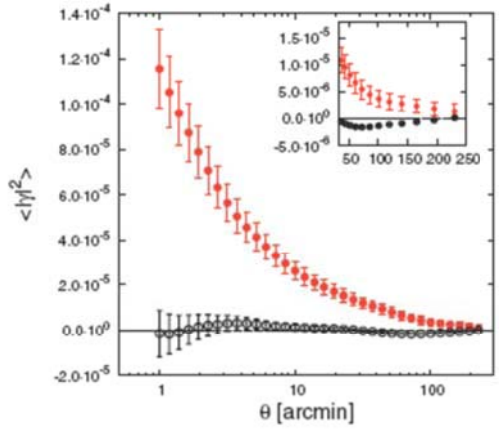

Fig. 4. Two-point statistics from the combined 57 pointings. The erro
bars of the E-mode include statistical noise added in quadrature to th
non-Gaussian cosmic variance. Only statistical uncertainty contribute
el show

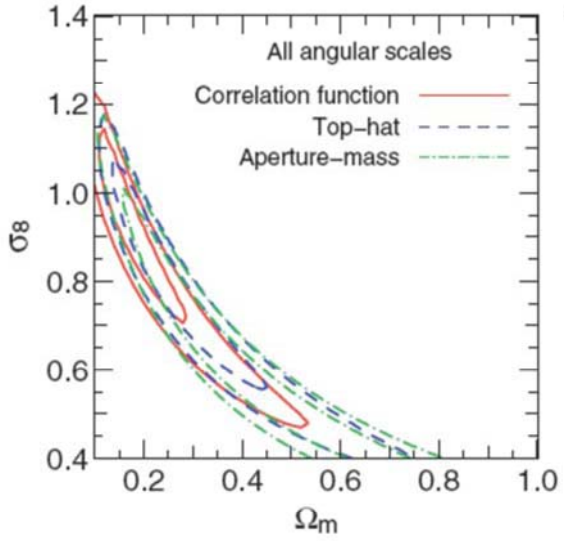

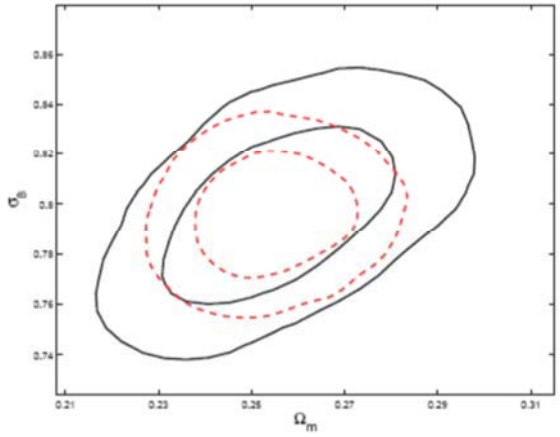

FIG. 1: Two dimensional constraints on σ_8 and Ω_m from the current observations in ΛCDM model, assuming a flat universe. The black solid lines are from data sets CMB + LSS + SN Ia and red dashed lines are obtained by taking into account the weak lensing data.

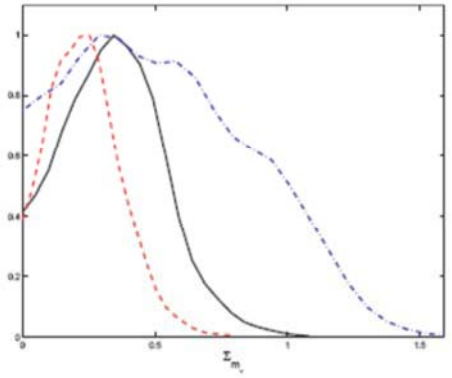

FIG. 2: one dimensional probability distribution of the total neutrino mass Σm_ν from the current observations assuming a flat universe. The black solid line is from data sets CMB + LSS + SN Ia, red dashed line is obtained by taking into account the weak lensing data and the blue dash-dotted line is for the dynamical dark energy model.

Current WL observations start to provide
useful complementary information
in constraining cosmological parameters

Current status

SDSS – large sky coverage, but very shallow $n_g \sim 1\, arc\,\mathrm{min}^{-2}$

CFHTLS – wide 172 deg^2, $n_g \sim 10\, arc\,\mathrm{min}^{-2}$

deep 4 deg^2, $n_g \sim 30\, arc\,\mathrm{min}^{-2}$

Subaru WL survey -- ~23 deg^2, $n_g \sim 15-50\, arc\,\mathrm{min}^{-2}$

COSMOS (HST) -- ~2 deg^2, $n_g \sim 70\, arc\,\mathrm{min}^{-2}$

PanSTARRS, DES, HSC, LSST, Euclid, WFIRST, KDUST, …

e.g., LSST: ~ wide-deep 18000 deg^2, $n_g \sim 40\, arc\,\mathrm{min}^{-2}$

Statistical power will increase enormously!

Current status

SDSS –

CFHTLS

Subaru

COSMO

PanSTARR

e.g., LSST:

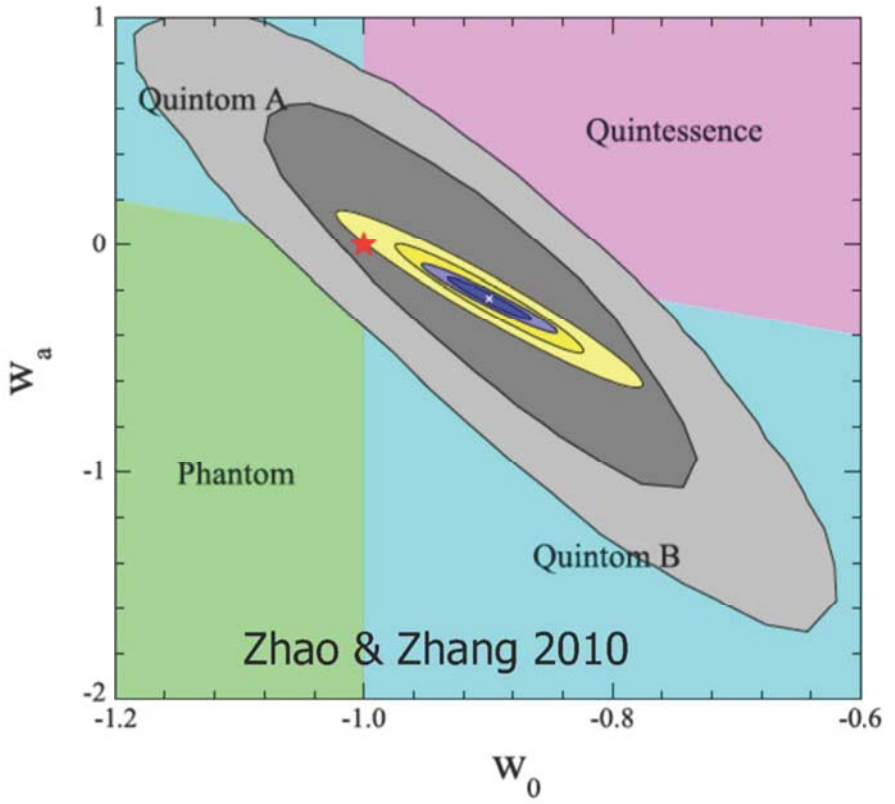

$\iota_g \sim 1\, arc\, \mathrm{min}^{-2}$

min^{-2}

T, ...

Statistical power will increase enormously!

Galaxy-Galaxy lensing

Munshi et al. 2008

Analyze weak lensing effects of background galaxies around foreground galaxies

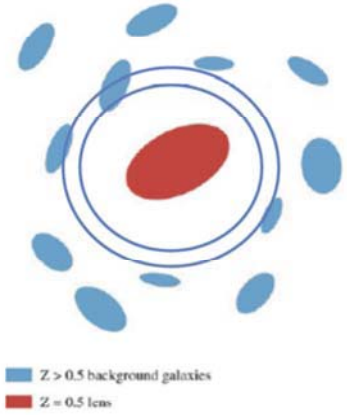

The signals around individual galaxies are very weak

→ stacking is needed to enhance S/N

→ statistically probe the mass distribution around foreground galaxies -- the galaxy-mass correlation

$$\Sigma(R) = \overline{\rho} \int \left[1 + \xi_{gm}\left(\sqrt{R^2 + \chi^2}\right)\right] d\chi$$

$$\Delta\Sigma(R) = \gamma_t(R)\Sigma_c = \overline{\Sigma}(< R) - \Sigma(R) \qquad \Sigma_c = \frac{c^2}{4\pi G}\frac{D_S}{D_L D_{LS}}$$

Munshi et al. 2008

galaxy scale: stack signals → galaxy-galaxy lensing

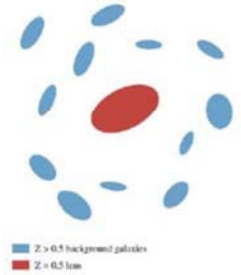

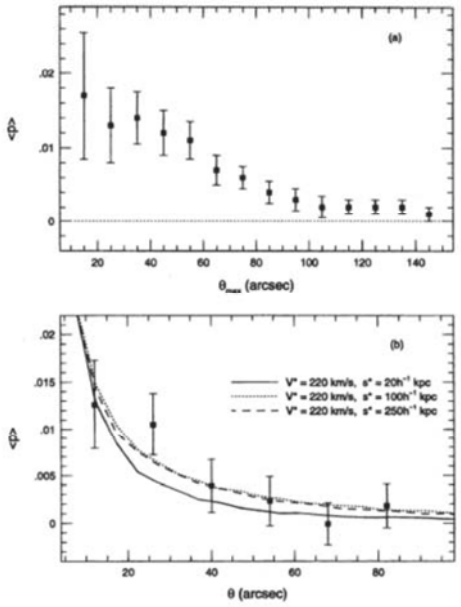

FIG. 5.—Angular variation of image polarization for foreground galaxies with $20 \le r_d \le 23$ and background galaxies with $23 < r_s \le 24$. (*a*) Variation of $\langle p \rangle$ with increasing annulus outer radius, θ_{max}. (*b*) Variation of $\langle p \rangle$ with differential lens-source separation, θ. Theoretical estimates of $\langle p \rangle$ (θ) for fiducial L^* galaxy gravitational lenses (see § 3) with different scaling radii, s^*, are also shown.

Brainerd et al. 1996, 5m Hale, Palomar

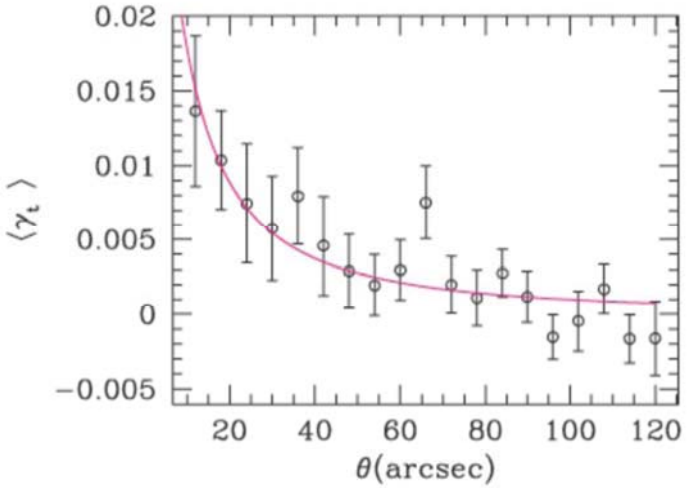

Figure 1. The average tangential alignment $\langle \gamma_t \rangle$ of source galaxies with respect to the lens sample as a function of angular separation on the sky θ. The solid curve shows the theoretical lensing signal from an NFW halo at $z = 0.65$, the median redshift of the lens sample, with the maximum likelihood method constrained virial radius $r_\Delta = 204\,h^{-1}$ kpc.

Heymans et al. 2006, HST GEMS

Divide foreground galaxies into different subsamples according to their properties: e.g., luminosity, color, etc.

→ stacked signals from different subsamples reveal the corresponding mass distributions

Munshi et al. 2008

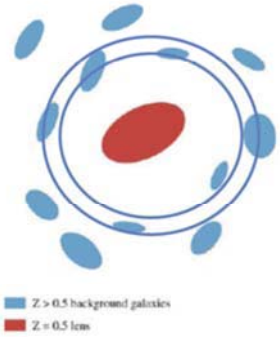

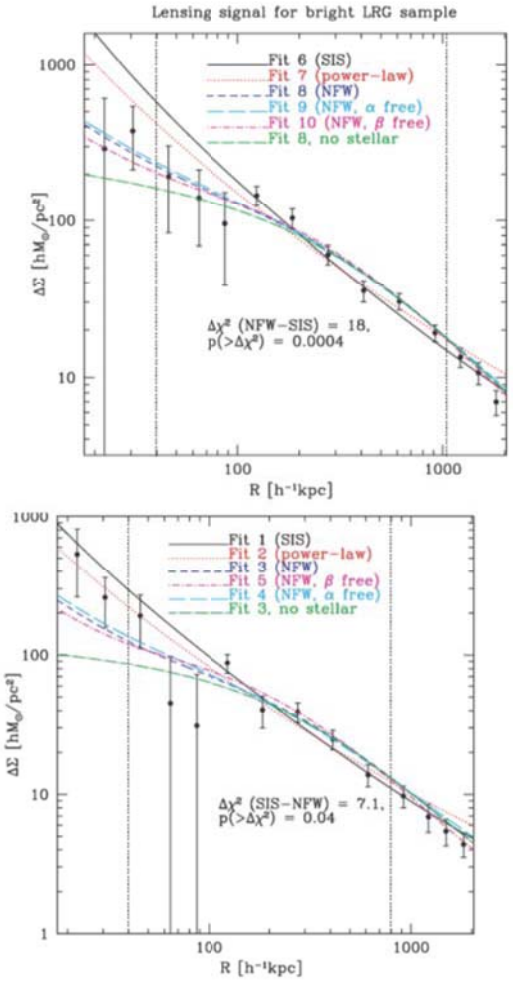

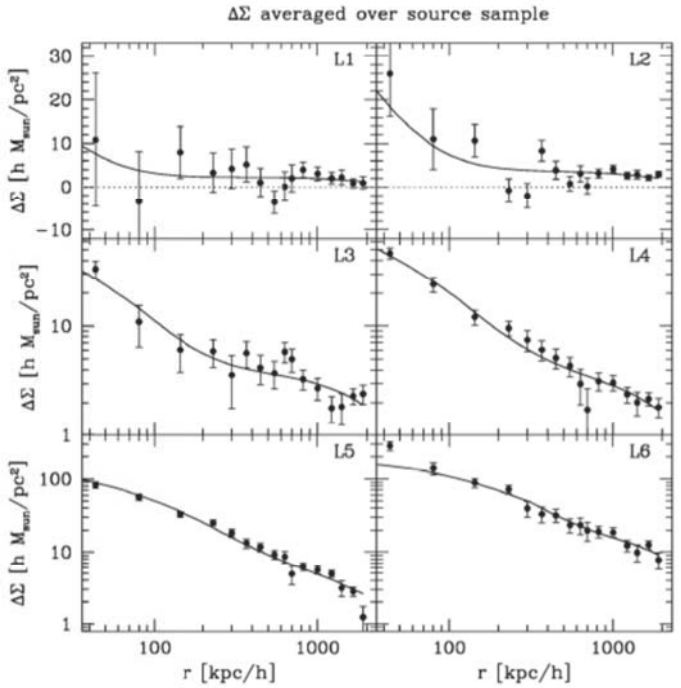

Figure 17. $\Delta\Sigma(r)$ averaged over source subsample as a function of lens luminosity. For L1 and L2, which have signal statistically consistent with zero, the vertical scale is not logarithmic, and the zero level is shown as a dashed line; for the other luminosity bins, a logarithmic scale is used for $\Delta\Sigma$. The error bars shown are statistical only; the lines are the results of halo model fits as described in the text.

Mandelbaum et al. 2006, SDSS

Confronted with dark matter halo models and cosmologies (Li et al. 2009, MNRAS)

Analyses are done with the information of galaxy group catalogs from SDSS (Yang, X. H. et al. 2007)

With the group catalog, we can separate central galaxies and satellite galaxies. The group catalog also provides a matched host dark matter halo mass to each group. Furthermore, we have the positions of the satellite galaxies and the mass of the associated subhalos can also be assigned according to certain ranking mechanism.

We then can model the g-g lensing signals taking into account different contributions from central and satellite galaxies without the need of using halo models, and further confront g-g lensing observations with cosmological models

The cosmological model from WMAP3 together with the NFW density profile for dark matter halos can give rise to g-g lensing signals that are in good agreements with SDSS observations. The model from WMAP1 (higher σ_8) over-predicts the signals.

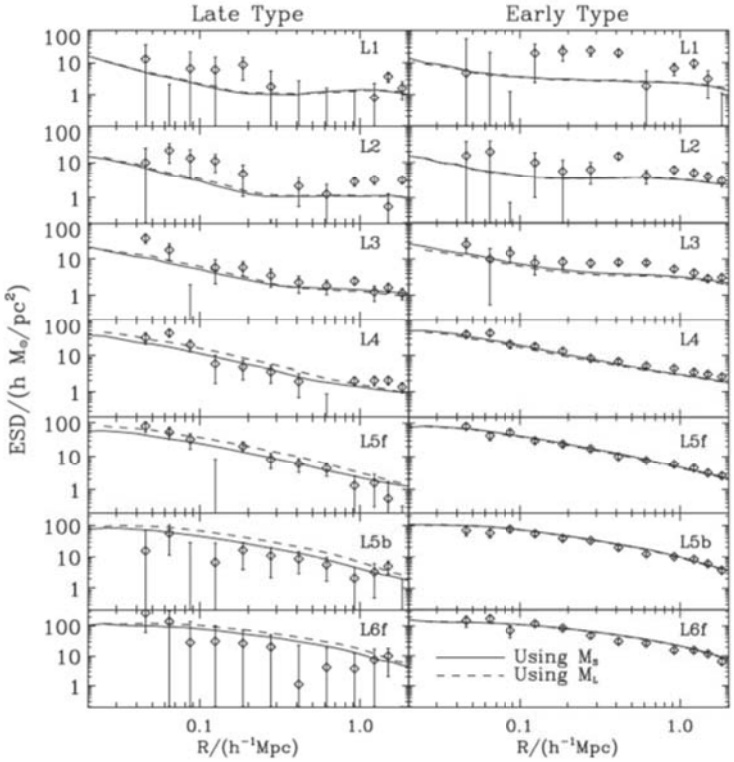

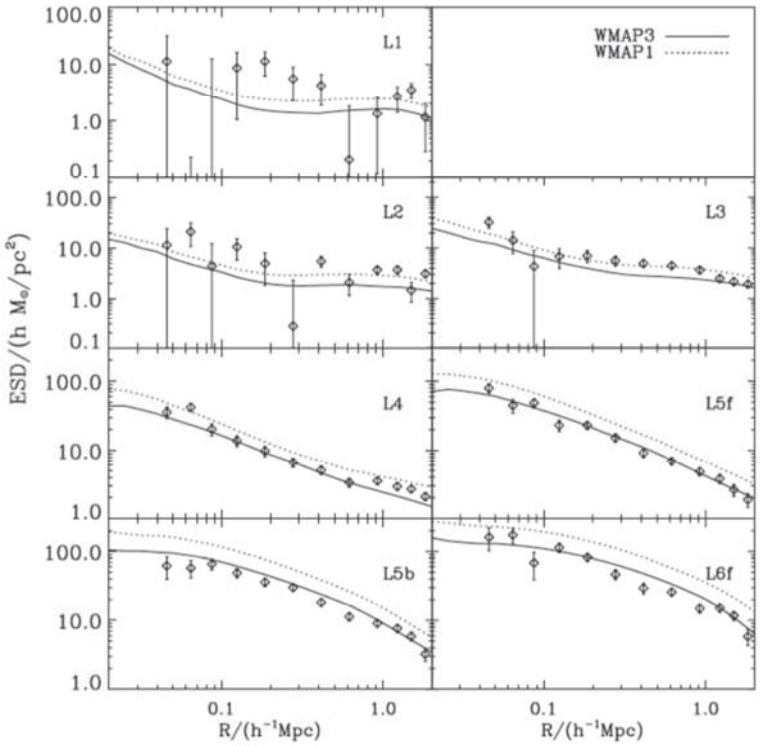

Li, R. et al. 2009, SDSS

- Probing subhalo mass distribution with future observations (Li et al. 2011)

Analyze the g-g lensing around satellite galaxies at a certain distance to the group center
(and a certain luminosity / stellar mass range)

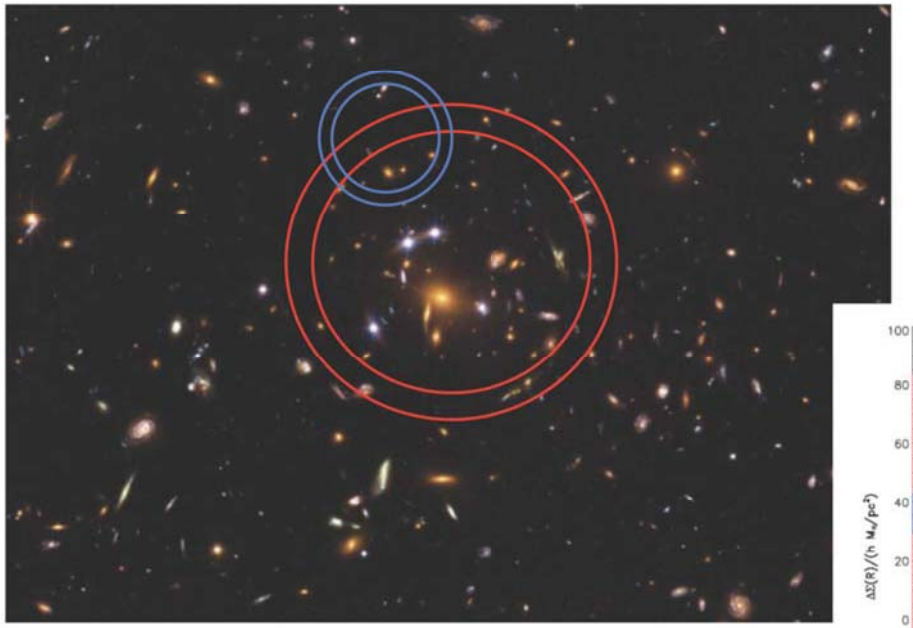

Figure 12.2: Lensed quasar SDS
http://hubblesite.org/newscen
LSST science book
). Shown is a color-composite
7]. The lens is a cluster of galax
five images with a maximum separation of 15 . LSST will act as a *finder* for exotic objects such a

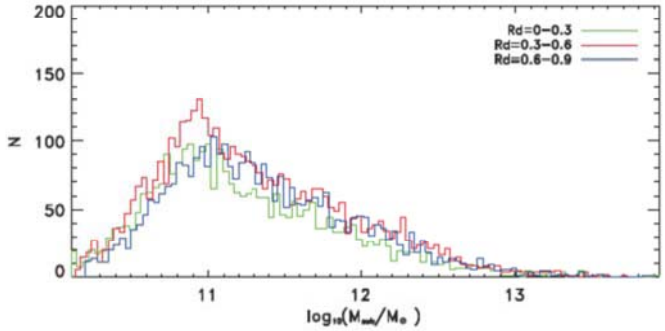

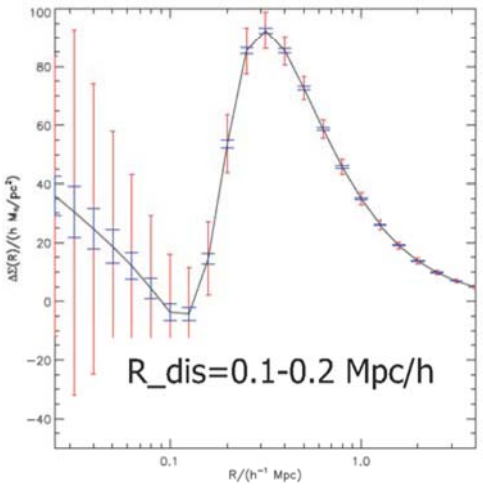

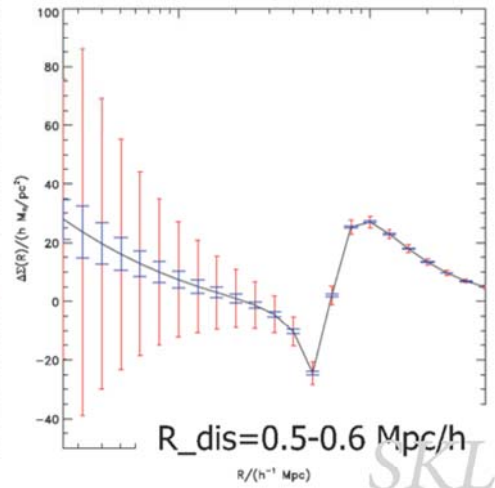

Table 1. show the mean value of parameters of the input galaxy sample, and the boundary of the flat prior we adopted in MCMC fitting. M and M_{sub} are in unit of $h^{-1}M_{\odot}$, $R_{\rm dis}$and $r_{\rm s,sub}$ are in unit of $h^{-1}Mpc$, $\rho_{0,\rm sub}$ is in unit of $10^{16}h^{2}M_{\odot}Mpc^{-3}$.

	$\lg M$	c	$R_{\rm dis}$	$\lg M_{\rm sub}$	$\rho_{0,\rm sub}$	$r_{\rm s,sub}$
mean input	14.1487	6.9	0.549	11.7	1.0	0.015
high bound	14.5	10	0.9	12.5	10	0.03
low bound	13.5	3	0.3	10.5	0.1	0.005

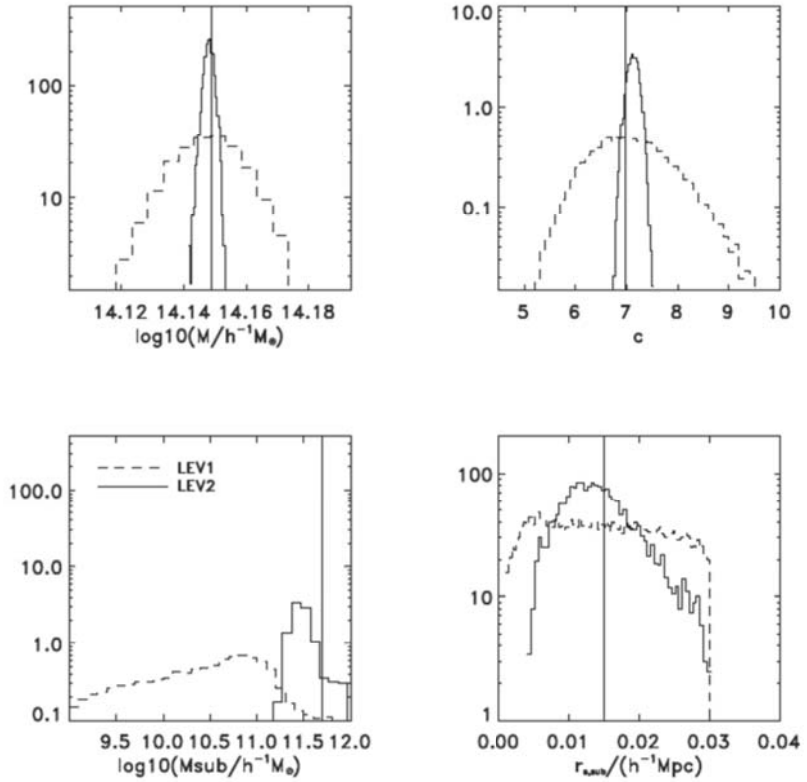

Figure 6. In this figure, we compares the parameter constrain under different noise level. The solid histograms show the marginalized probability distribution of M, c, $M_{\rm sub}$ and $r_{\rm sub}$ for LEV2 case, while the dashed histograms for LEV1 case.

MCMC analyses

LEV1: SDSS $n_g = 1\ arc\min^{-2}$

LEV2: LSST $n_g = 60\ arc\min^{-2}$

Number of groups is the same as that of SDSS

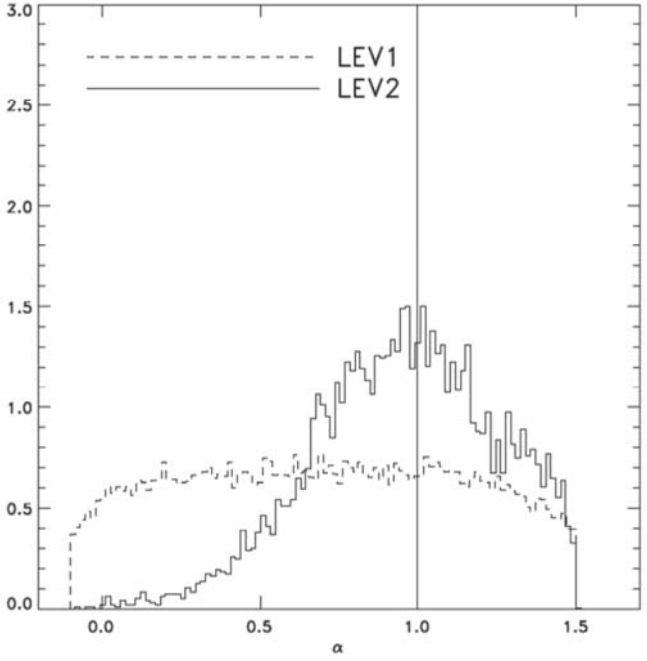

Inner density slope of subhalos

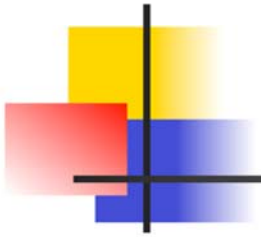

Current g-g lensing from SDSS cannot have any meaningful constraints on subhalo properties (e.g., M_{sub}, $r_{s,sub}$, α)

LSST will have the potential to provide much tighter constraints on these quantities

* We are investigating different systematics.

satellite contamination

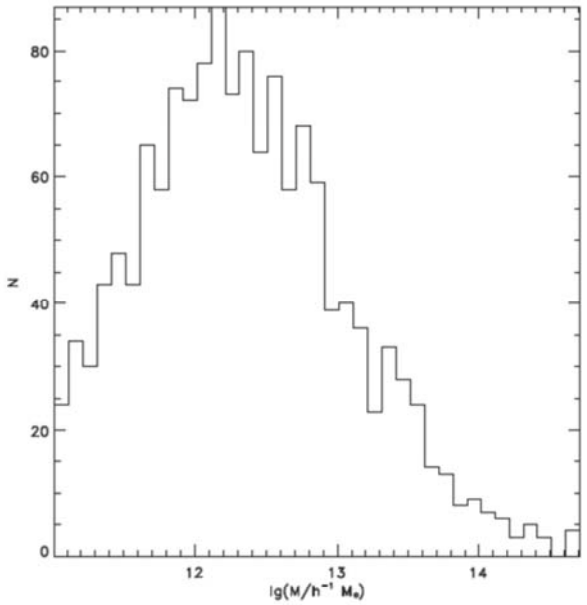

Figure 1. The histogram shows the halo mass distriubtion of fake memebers which are assigned groups in mass bin of $[10^{14}, 2\times 10^{14}]h^{-1}M_{\odot}$.

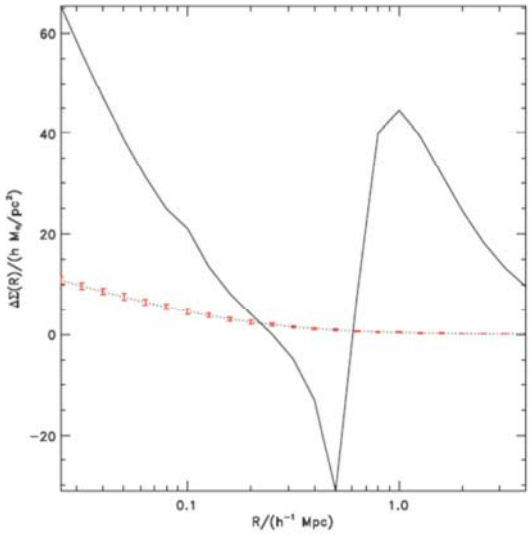

Figure 2. The figure shows the lensing signal from true satellites (solid) and that from fake members. The galaxies are selected to be in halo of $[10^{14}, 2\times 10^{14}]h^{-1}M_{\odot}$ and halo-centric radius of $[0.5, 0.6]h^{-1}Mpc$. We show the standard deviation of fake members contamination with errorbar.

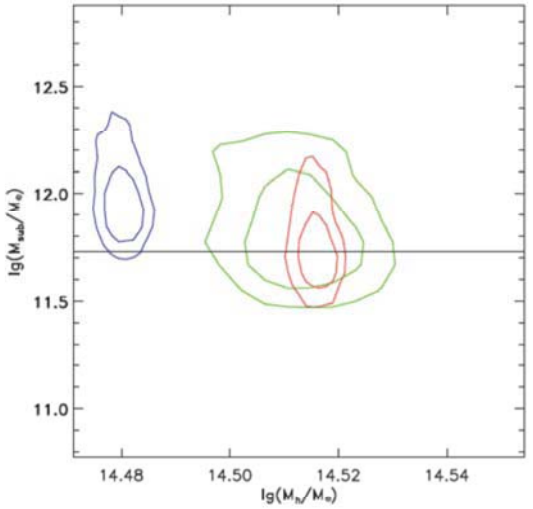

Figure 3. In Fig.3, we show the constraints on host halo mass and subhalo mass. The blue contours show the result by using the mixed signal. The red contours show the constraints from true signal which is calculated using only true satellites. And the green contours show the constraints from corrected signal. The black solid lines shows the value of input satellite mass.

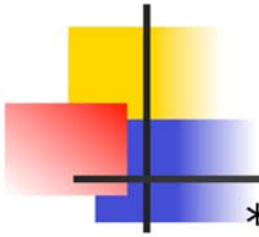

* The analyses still use SDSS group catalog. LSST will generate their own group catalog based on photo-z. Applying the g-g subhalo analyses to groups at different redshifts, we can potentially probe the time-dependence of the subhalo properties. On the other hand, groups identified based on photo-z can have larger contamination fraction, and their effects need to be carefully studied.

Weak-lensing peak statistics

Weak lensing observations can give rise to large-scale projected mass distribution, allowing for blind detection of clusters of galaxies. The peak abundance carries important cosmological information.

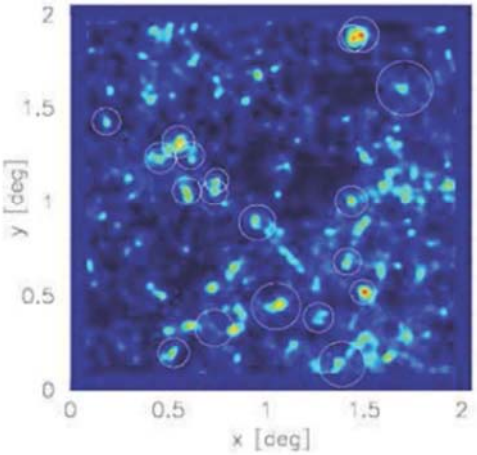

M. White et al. 2002
T. Hamana et al. 2004
Tang & Fan 2005

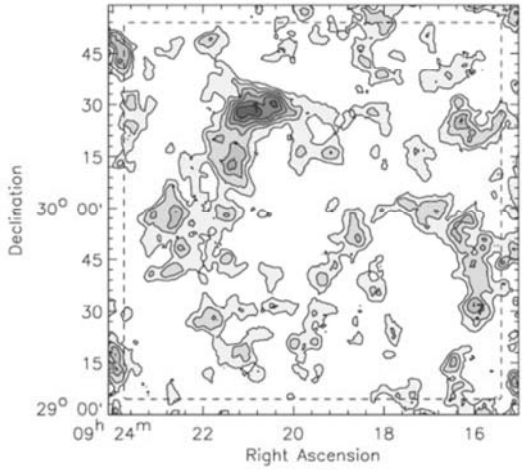

Fig. 3.—C convergence i indicates high exclusion zon a. For all ity, black e 5′ edge

Wittman et al. 2006
Deep Lens Survey

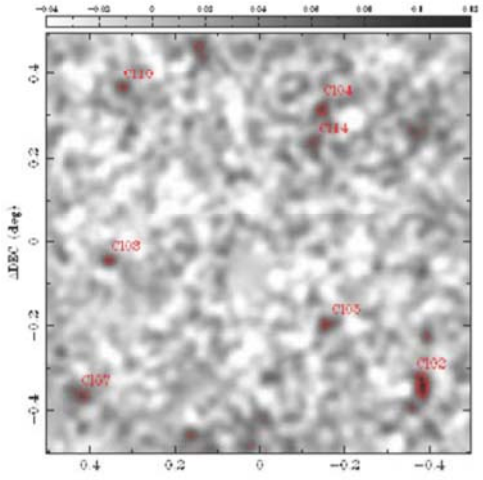

Gavazzi & Soucail 2006
CFHTLS Deep

Peaks in the projected mass map ⟷ ?? 3-d mass concentrations
(clusters of galaxies)

projection effect along the line of sight (correlated/uncorrelated)

intrinsic ellipticities of source galaxies

generate false peaks
(with respect to the peaks from true halos)
affect the peak height
and position of the true peaks

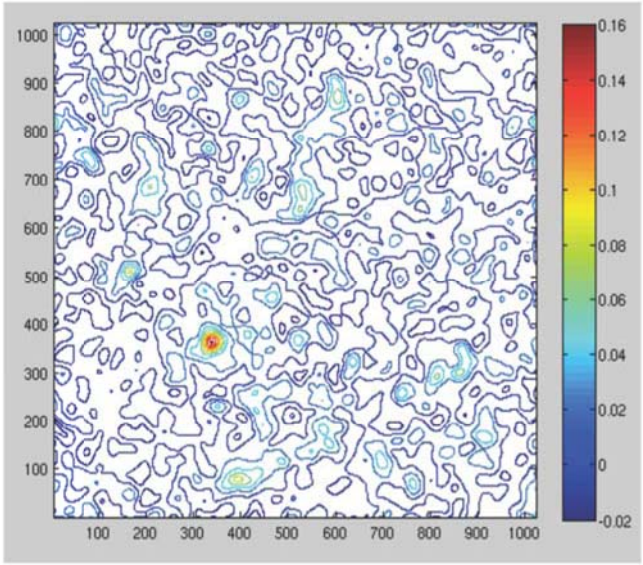

(Fan et al. 2010) In the weak lensing regime,

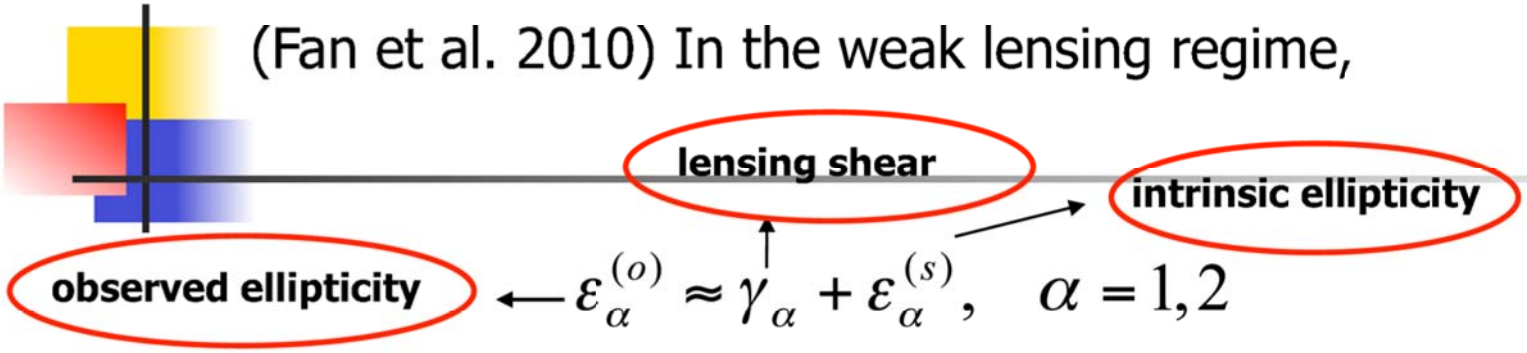

$$\kappa_n(\mathbf{k}) = c_\alpha \varepsilon_\alpha^{(o)} = \kappa(\mathbf{k}) + c_\alpha \varepsilon_\alpha^{(S)}, c_\alpha = [\cos 2\varphi, \sin 2\varphi] \quad \mathbf{k} \approx k[\cos\varphi, \sin\varphi]$$

Smoothed shear and convergence

$$\Sigma_\alpha^{(O)}(\boldsymbol{\theta}) \approx \Gamma_\alpha(\boldsymbol{\theta}) + \Sigma_\alpha^{(s)}(\boldsymbol{\theta}) = \Gamma_\alpha(\boldsymbol{\theta}) + \frac{1}{n_g}\sum_{i=1}^{N_g} W(\boldsymbol{\theta} - \boldsymbol{\theta}_i)\varepsilon_\alpha^{(s)}(\boldsymbol{\theta}_i), \quad \alpha = 1,2$$

$$\mathrm{K}_N(\boldsymbol{\theta}) = K(\boldsymbol{\theta}) + N(\boldsymbol{\theta}) = \int d\mathbf{k} \exp(-i\mathbf{k} \bullet \boldsymbol{\theta}) c_\alpha(\mathbf{k}) \Sigma_\alpha^{(o)}(\mathbf{k})$$

** Note for the peak statistics,

$$N_{peak}(K_N) \neq N_{peak}(K) + N_{peak}(N)$$

Peak statistics near halo regions

known halo profile

$$K_N(\vec{\theta}) = K(\vec{\theta}) + N(\vec{\theta})$$ → Gaussian noise field

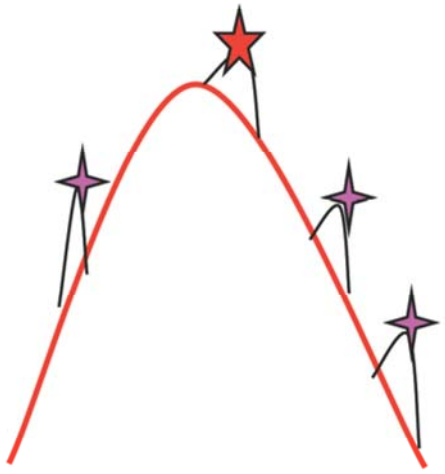

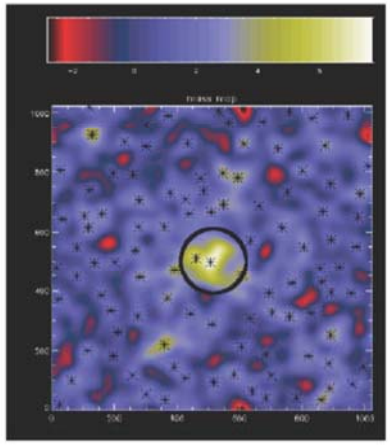

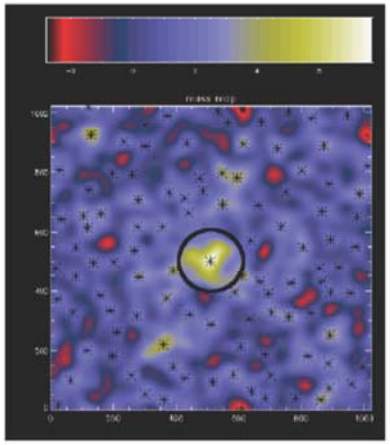

** The number density of noise peaks is strongly enhanced in the halo region → depends on the density profile of the halo → noise peaks carry cosmological information

Both the position and the height of the halo peak are affected by noise

Halo peak position

$$p(\Delta R)d\Delta R \approx \frac{2\pi\Delta R d\Delta R \int n_{peak}(\Delta R,\nu)d\nu}{[\int_0^{R_c} d\Delta R(2\pi\Delta R)\int n_{peak}(\Delta R,\nu)d\nu]}$$

$$p(\Delta R)d\Delta R \approx d\Delta R \frac{\Delta R \exp\{-[K^{11}(0)\Delta R/\sigma_1]^2\}}{\int_0^{R_c} d\Delta R\ \Delta R \exp\{-[K^{11}(0)\Delta R/\sigma_1]^2\}]}$$

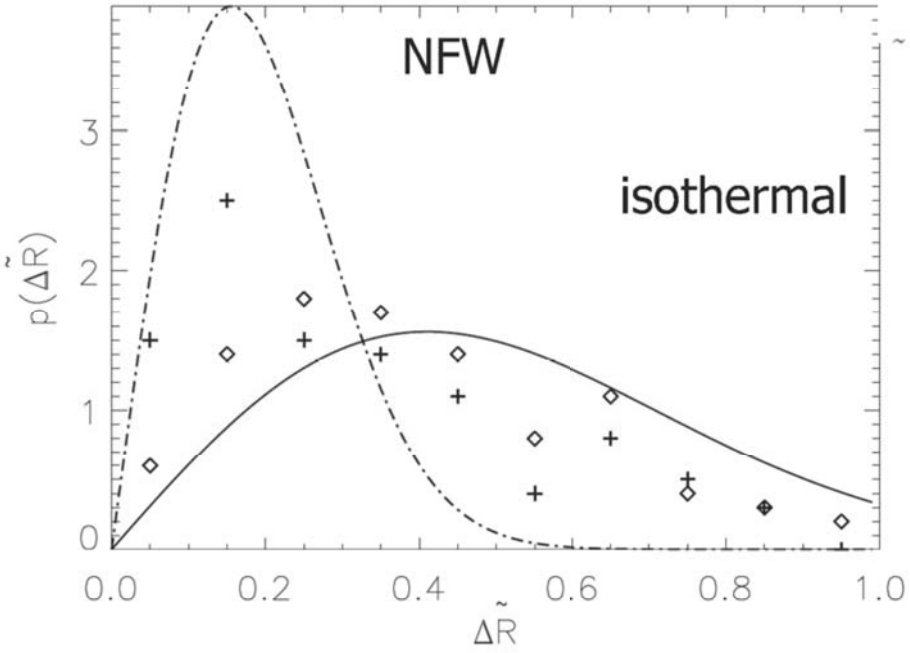

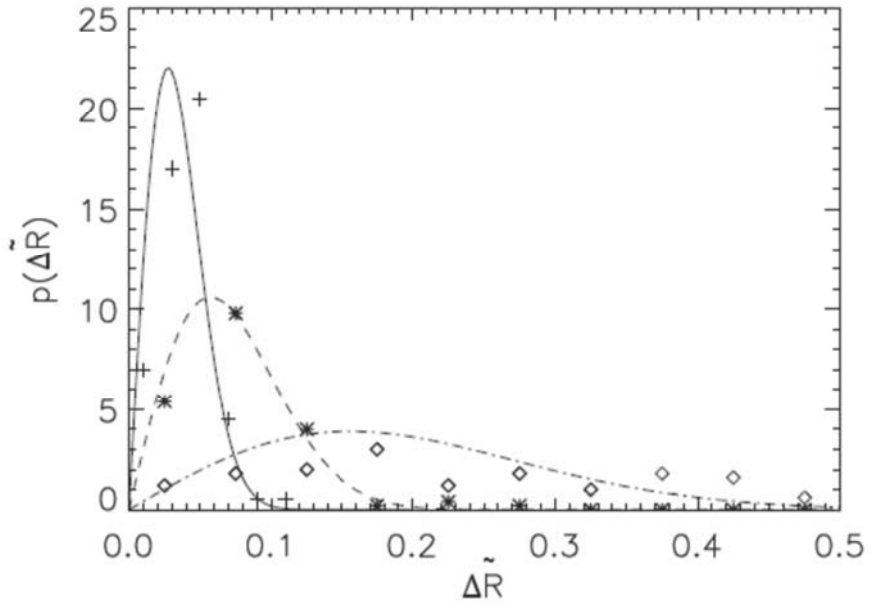

Fig. 8.— The spatial offset distribution of the measured main-cluster-peak position tc ... true center of the cluster. The solid and dash-dotted lines ar Eq. (34) for the isothermal cluster and the NFW cluster, plus symbols are for the corresponding results from Monte parameters are the same as those in Figure 2.

The more centrally concentrated the profile is, the smaller the offset ΔR is.

Halo peak height

$$p(\nu) = \frac{n_{peak}(\nu)}{[\int n_{peak}(\nu')d\nu']}$$

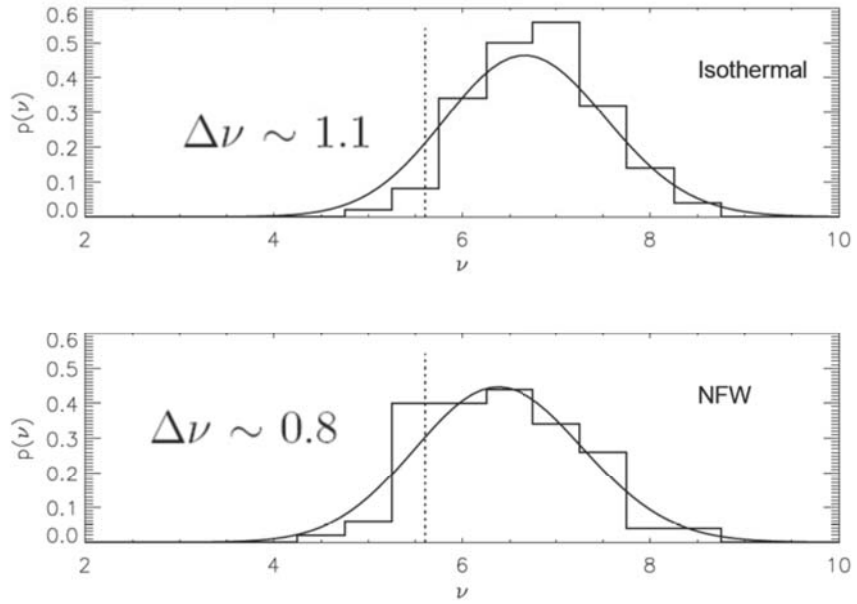

Fig. 7.— The height distribution of the main-cluster-peak measured from noisy weak-lensing convergence maps. The upper and the lower panels are for the isothermal and the NFW clusters, respectively. The solid line in each panel is for the result calculated from Eq. (31). The histogram is for the result from our Monte Carlo simulations. The vertical dotted line indicates the value of $\nu = 5.6$, the true peak height of the considered cluster. The cluster parameters are the same as those in Figure 2.

The more centrally concentrated the profile is, the smaller Δv is.

K, K^1, K^2, K^{11} and K^{22} at $\tilde{R} = 0$

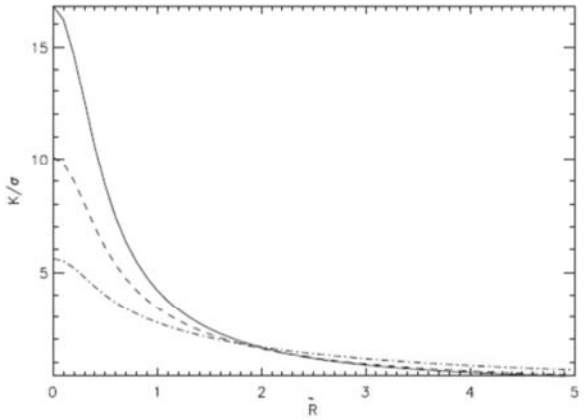

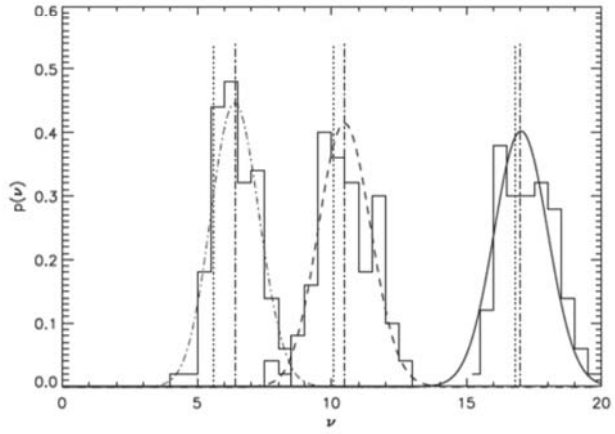

Statistical peak abundances over a large field

Halo region + field region

$$n_{peak}(\nu)d\nu = n^{c}_{peak}(\nu)d\nu + n^{n}_{peak}(\nu)d\nu$$

$$n^{c}_{peak}(\nu) = \int dz \frac{dV(z)}{dz d\Omega} \int dM\, n(M,z)\, f(\nu, M, z)$$

$$f(\nu, M, z) = \int_0^{R_{vir}} dR\ (2\pi R)\ n_{peak}(\nu, M, z)$$

$$n^{n}_{peak}(\nu) = \frac{1}{d\Omega}\left\{ n_{ran}(\nu)\left[d\Omega - \int dz \frac{dV(z)}{dz} \int dM\ n(M,z)\ (\pi R^2_{vir}) \right] \right\}$$

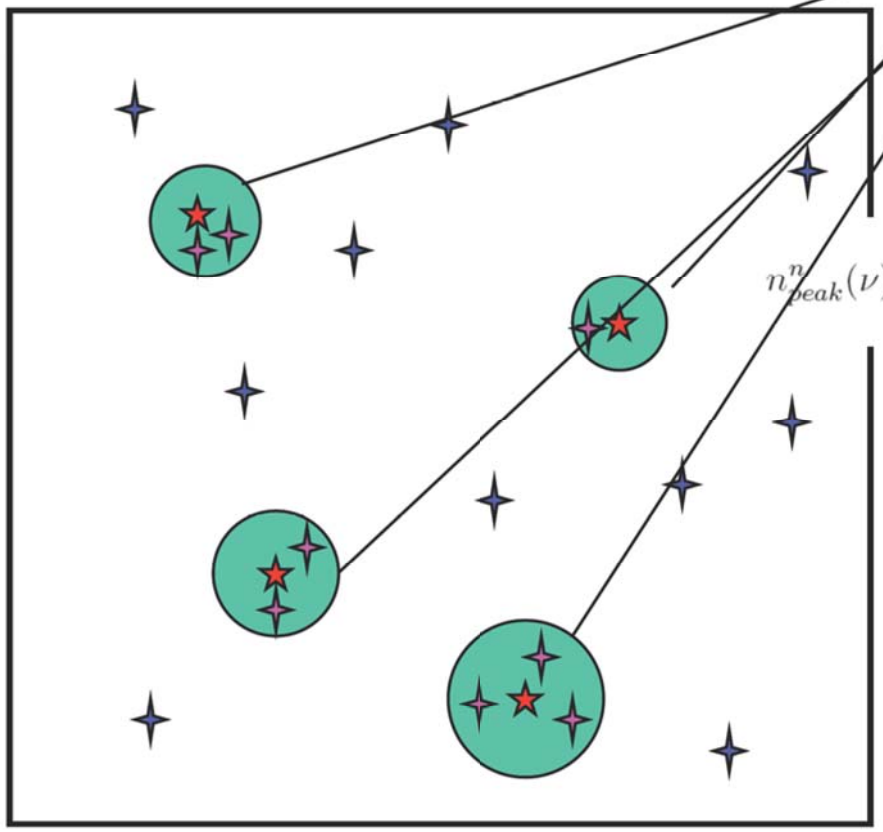

Halo region:

** Halo peak is affected by noise
** Number of noise peaks is enhanced by the halo mass distribution

Comparison with simulations

(*http://mwhite.berkeley.edu/Lensing*)

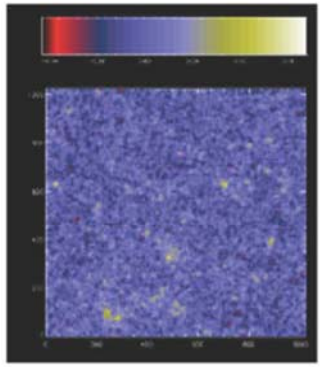

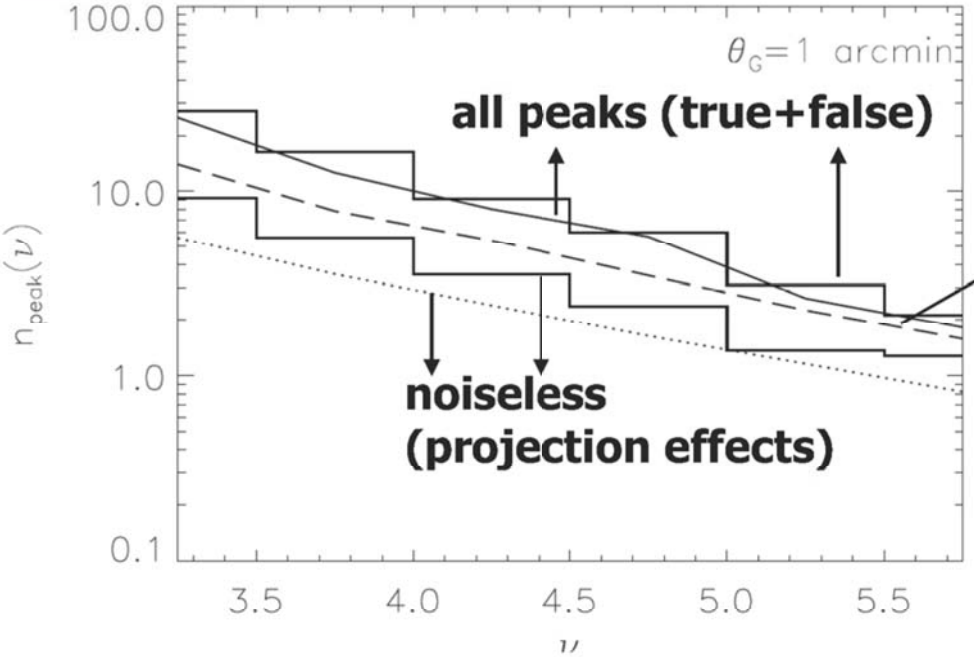

Effect on halo peak height

$$n_{peak}(\nu) = \int dz \frac{dV(z)}{dz d\Omega} \int dM\ n(M,z)\ p_{peak}(\nu, M, z)$$

$$p(\nu) = \frac{n_{peak}(\nu)}{[\int n_{peak}(\nu')d\nu']}$$

Fig. 10.— The differential peak height distribution in 1 deg^2. The histograms are for the results averaged over 16 ray-tracing simulations with 3×3 deg^2 each by White and Vale (2004). The lower and upper histograms correspond to the results without and with noise included. The dotted line is for [illegible] ering only NFW halos without noise [Eq. (40)]. The long-dashed line is for the result of dark matter halos including the noise effects on the their peak heights calculated from Eq. (41) and Eq. (31). The solid line is for the prediction from Eq. (35)-Eq. (38) including the full noise effects.

Fan et al. 2010

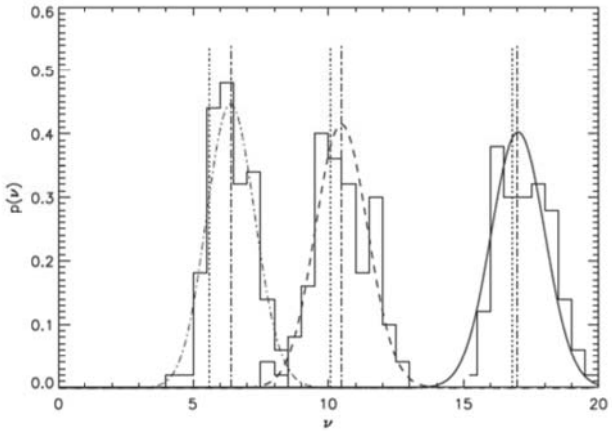

Shan et al. 2011, mass distribution from CFHTLS 72 deg^2

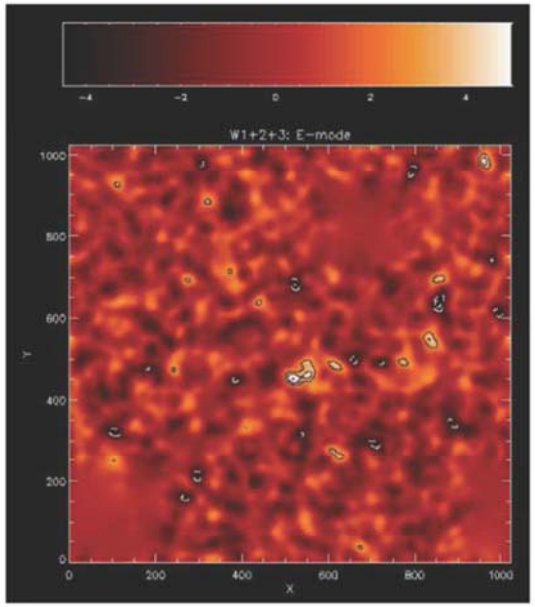

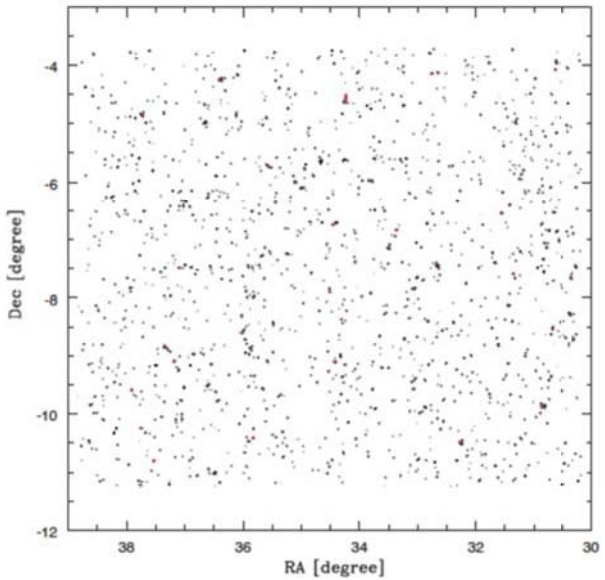

Figure 12. Reconstructed "dark matter mass" convergence map for the entire CFHTLS Wide W1 field. The smoothing scale $\theta_G = 1'$. The lowest contour is drawn at detection signal-to-noise ratio $\nu = 3.0$, and successive contours are drawn in increments of $\Delta\nu = 0.5$. The red contours denote $\nu \geq 4.5$.

peak statistics

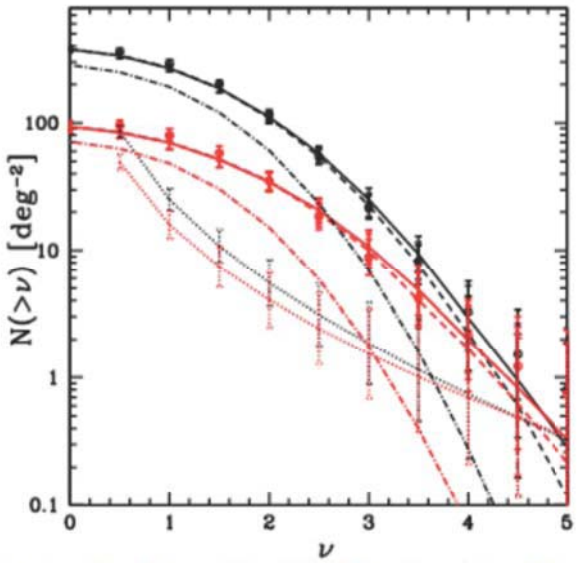

Figure 14. Cumulative density of local maxima $N(> \nu)$ (solid line) and corresponding density of local minima $N(< -\nu)$ (dashed line) in the CFHTLS-Wide W1 E-mode (top-panel) and B-mode (bottom-panel) convergence map with smoothing scale $\theta_G = 1'$ (black) and $\theta_G = 2'$ (red). Error bars are simply 1σ uncertainties assuming Poisson shot noise. The dot-dashed line shows the prediction from Gaussian random field theory (van Waerbeke 2000). Circles with additional error bars and the dotted curves show an analytical prediction in a ΛCDM universe (Fan et al. 2010), with and without the influence of random noise. The excess of positive maxima over negative minima demonstrates the non-Gaussianity of the convergence field.

Statistical peak abundances

Develope a HOD-like model to calculate the total peak abundances:

halo mass function, halo density profile

halo peak height change, noise peak enhancement

We can then use the total number of peaks in convergence maps (true + false) for cosmological studies without the need to differentiate true and false peaks

Considering only true peaks, our model can correctly calculate the the shift and the scatter of the peak height due to noise. Without such analyses, we expect large biases on cosmological parameters inferred from observed weak-lensing cluster abundances.

LSST will be able to detect much more peaks, and thus is expected to provide important cosmological constraints compliment to two-point correlation analyses of cosmic shear.

Systematic effects must be thoroughly investigated

** Projection effects of large-scale structures

$$K_N = K + K_{LSS} + N$$

K_{LSS}: in linear regime --> Gaussian random field,
then our model can be readily extended to include the projection effects

However: non-linear K_{LSS} , correlation between K and K_{LSS}
(e.g., Yan and Fan 2011: filaments statistics)

** Effects of masks on the peak statistics

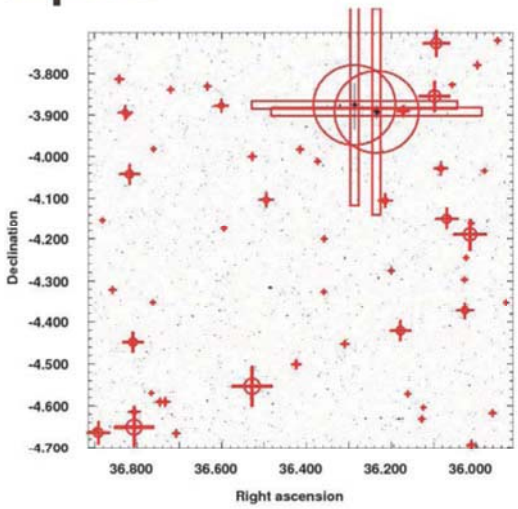

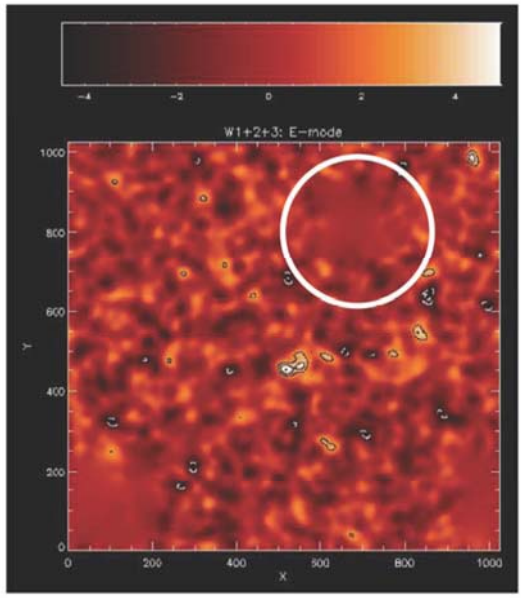

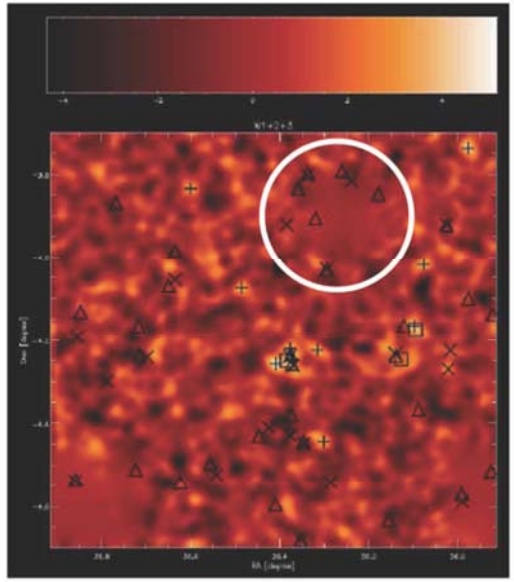

Shan et al. 2011, CFHTLS

LSST will be able to probe small-scale structures.
Masks can have more significant effects on peak statistics than those for CFHTLS analyses

galactic scale – galaxy-galaxy lensing
cluster scale – individual studies, statistical analyses
large-scale structures – cosmic shear

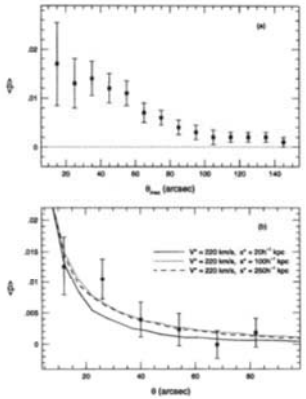

Brainerd et al. 1996, 5m Hale, Palomar

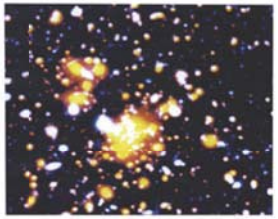

Tyson et al. 1990

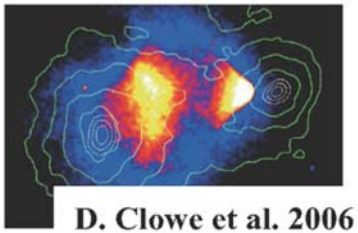

D. Clowe et al. 2006

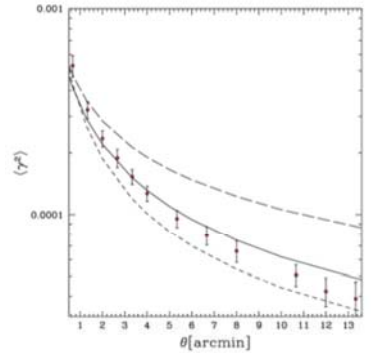

Van Waerbeke et al. 2001 A&A (VIRMOS (CFHT), ~6.5 sq. deg)

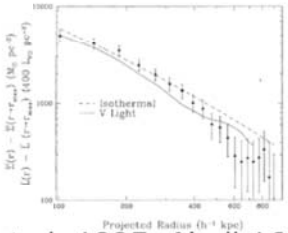

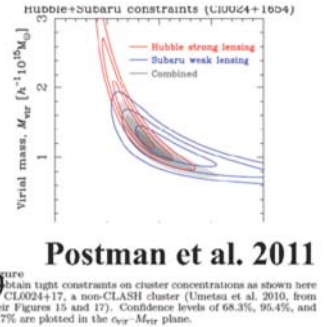

Tyson et al. 1995, Abell 1689

Postman et al. 2011

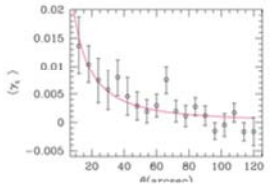

Heymans et al. 2006, HST GEMS

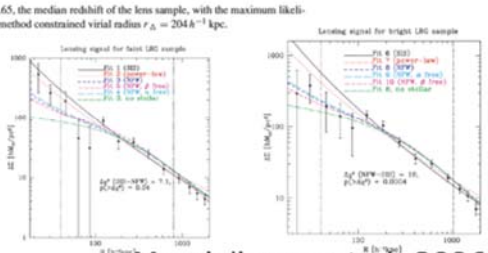

Mandelbaum et al. 2006, SDSS

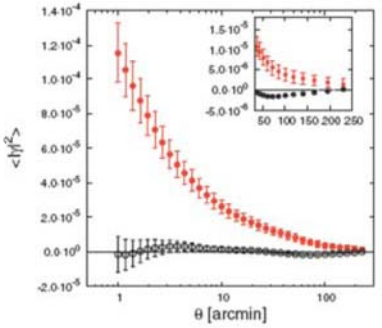

Fu et al. 2008 A&A (CFHTLS, 57 sq. deg)